Received February 14, 2019, accepted February 27, 2019, date of publication March 4, 2019, date of current version March 20, 2019.

Digital Object Identifier 10.1109/ACCESS.2019.2902956

Advanced Filtering Solutions in Coaxial SIW Technology Based on Singlets, Cascaded Singlets, and Doublets

STEFANO SIRCI[1], (Member, IEEE), MIGUEL ÁNGEL SÁNCHEZ-SORIANO[2], (Member, IEEE), JORGE DANIEL MARTÍNEZ[3], (Member, IEEE), AND VICENTE E. BORIA[1], (Fellow, IEEE)

[1]Institute of Telecommunications and Multimedia Applications, Universitat Politècnica de València, 46022 Valencia, Spain
[2]Department of Physics, Systems Engineering and Signal Theory, University of Alicante, 03690 Alicante, Spain
[3]I3M, Universitat Politècnica de València, 46022 Valencia, Spain

Corresponding author: Stefano Sirci (ssirci@iteam.upv.es)

This work was supported by the Ministerio de Economía, Industria y Competitividad, Spanish Government, under Project TEC2016-75934-C4-3-R.

ABSTRACT The use of singlets, cascaded singlets, and doublets in a coaxial substrate integrated waveguide (SIW) technology is proposed in this paper, with the aim of implementing low-loss filters with very compact size and highly selective symmetric, asymmetric as well as dual-band responses. Singlets based on coaxial SIW resonator structures with source-load coupling are presented and studied. Then, different filter examples based on N cascaded singlets are designed, fabricated, and measured at 7.5 GHz, with up to N transmission zeros that can be easily located below and above the passband. Moreover, the application of doublets based on a dual-mode coaxial SIW resonator with source-load coupling for achieving extremely compact dual-band filters is presented, and two examples with different bandwidth configuration for each channel are designed, demonstrating the flexibility of the proposed coaxial SIW structure. The obtained experimental results of the differently implemented filters show a good agreement with simulations, thus confirming the interesting potential application of these structures for the design of very compact devices with advanced filtering responses.

INDEX TERMS Band pass filters, cavity resonators, bypass coupling, cross coupling, elliptic filters, microwave filters, resonator filters, singlets, substrate integrated waveguide (SIW), transmission zero.

I. INTRODUCTION

The design of high selectivity filters have usually relied on the introduction of transmission zeros (TZs) at finite frequencies. Different techniques have been extensively researched with this goal. These include the introduction of cross-couplings between non-adjacent resonators, which has been broadly explored in waveguide [1], [2], planar [3], [4] and substrate integrated waveguide (SIW) technologies [5]–[10], or the use of extracted-pole synthesis methods in order to produce asymmetric responses with flexible allocation of TZs [11]. Together with the former considerations, there is also an increasing need of further reduction on the size and cost of microwave filters, as well as providing extra functionalities like frequency tuning [12], filter response reconfiguration [13] or multi-band operation [14], [15]. And this is imposing additional constraints on the previously indicated filter topologies. They are not always well-suited for satisfying the new demands on small size and low complexity filters, due to the complicated routing schemes involved, the dispersive behavior of mixed electric and magnetic couplings, and the extra size required for pole extraction.

Singlets, cascaded singlets and doublets are also extremely useful building blocks for compact high-selectivity microwave filters [16]–[19]. These topologies enable us to design filtering responses having N TZs with N resonant elements by providing additional paths between source and load. Thus, the synthesis of advanced filtering responses can be easily achieved by using non-resonating nodes (NRN) to cascade N singlets.

In this context, the definition of singlet was firstly envisaged in [16], where it was defined as the most basic building block for modular design of elliptic filters that contains

The associate editor coordinating the review of this manuscript and approving it for publication was Lin Peng.

one resonator and generates one TZ. Indeed, the idea of exploiting additional couplings between the source-load and resonators to generate N finite TZs with N resonators had been proposed by Amari *et al.* [20], where a comprehensive synthesis technique of coupled resonator filters with source/load-multiresonator coupling is shown.

However, such interesting structures have not been extensively reported in SIW technology [18], [19], [21]. For instance, cascaded singlets based on oversized SIW cavities have been just recently proposed for implementing dual-band band-stop filters [18]. Furthermore, SIW mushroom-shaped resonators have been also used for implementing quasi-elliptic filters [19], although at the cost of a more complex manufacturing process and lower EM performance. Finally, in conventional dual-mode SIW filters, the interaction of the coupling ports and the location of a perturbation via introduced at the SIW cavity corner has been investigated to introduce multiple TZs at one side or both sides of the passband [21]. Note that, in this approach, to provide multiple paths, the fundamental TE_{101} mode plays the role of NRN. Even if a more flexible design and enhanced performance responses are achieved, filter miniaturization cannot be easily implemented using the proposed approach.

In this context, coaxial SIW structures present important advantages for implementing filters with advanced responses due to their low loss, compact size, tuning capabilities and easy integration. Thus, the use of cascaded singlets in coaxial SIW has been already demonstrated in [22] for the introduction of TZs below the passband, generating highly-selective asymmetric responses. Moreover, doublets based on dual-mode coaxial SIW resonators were also proposed in the same work for the design of quasi-elliptic single band filters. In this paper, the concept of coaxial SIW singlet is generalized and extended in order to be able to locate the TZ selectively below or above the passband, by using electric and magnetic coupling for the source-load path of the structure. Such building block can then be used to perform filters with symmetric quasi-elliptic response, or asymmetric responses with steep filter skirts, based on cascaded singlets. In addition, the proposed approach is also here extended to the dual-mode coaxial SIW cavity [23] with the aim of designing highly-selective dual-band filters with a high degree of miniaturization.

To validate the proposed topologies, several filter designs are shown in the following Sections. First, Section II presents the working principles of the proposed coaxial SIW singlets. Then, in Section III, two different filter examples using two cascaded singlets are presented, showing different distributions of the TZs below and above the passband. Moreover, a filter with three cascaded singlets is also presented showing that this structure can be easily scaled. Finally, in Section IV, the design of a novel dual-band topology based on coaxial SIW doublet is proposed and experimentally demonstrated by means of different filter examples.

II. SINGLET IN COAXIAL SIW

Fig. 1 shows the routing schemes of a singlet, where grey numbered circles are resonator nodes, S, L and m_{s1} stand for source port, load port and main direct coupling, respectively. Finally, m_{sl} represents the cross coupling, which can be based on an electric (dashed line) or magnetic (solid line) coupling mechanism.

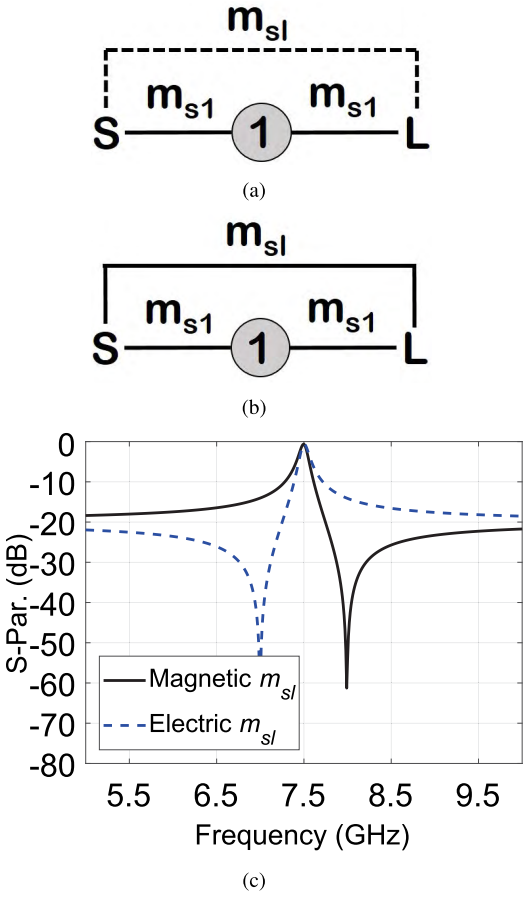

FIGURE 1. Routing scheme of a singlet with: (a) negative (electric) and (b) positive (magnetic) source/load coupling. (c) Synthesized frequency responses of both singlets.

As firstly demonstrated in [16], the singlet consists of a first order topology able to produce a TZ either below or above the transmission pole. Indeed, the singlet provides two possible paths that connect the source and the load: the main path *S-1-L* and the direct path *S-L*. This filtering configuration has been widely studied and validated with different technological realizations; for instance using planar circuits [16], classical waveguide [17], [24], and more recently SIW technology [18], [19], [22].

The objective of this work is to implement singlet topologies in SIW technology that are able to generate TZs in a flexible way whereas keeping very compact size, low-cost batch fabrication, and moderate-to-high unloaded quality factor (Q_u). Hence, the direct path *S-L* is chosen to be implemented by means of an embedded direct bypass coupling.

This is in contrast to the approach used in previous works, such as [18], where higher order modes excited in oversized SIW cavities are providing the direct source-load coupling, with a cost in terms of filter miniaturization.

Using the approach proposed in [2] to illustrate the introduction of TZs in coaxial cavity resonator filters, the working principle of the singlet can be explained looking at the phase shift of the two possible signal paths. When this phase shift is approaching 180°, an out of phase condition is achieved, thus a destructive interference between the signal paths generates a TZ in the frequency response. In this context, let us view the singlet as a two-port device, and, as proved in [2], let us consider that:

- If the input signal is below the resonant frequency f_0, thus below the passband, the phase shift introduced by the resonator is approaching $+90°$. In the case of input above f_0, the phase shift tends toward $-90°$.
- Electric (negative) coupling mechanisms, which are represented by series capacitors, provide a $+90°$ phase shift to the incoming signal.
- Magnetic (positive) coupling mechanisms, which are represented by series inductors, provide $-90°$ phase shift to the incoming signal.

Since an embedded direct source/load coupling m_{sl} is now used to provide the direct path for signal passing through the singlet, the position of the TZ only depends on the sign of the bypass coupling m_{sl}, thus on the type of coupling mechanism that is chosen. Indeed, if m_{sl} is electric, the TZ appears below the passband because the two paths are out of phase below f_0 (i.e. the phase shift of the path S-1-L with electric m_{s1} is $+90° + 90° + 90° = +270°$ or, with magnetic m_{s1} is $-90° + 90° - 90° = -90°$, whereas in the direct path S-L is always $+90°$). On the contrary, a magnetic m_{sl} is responsible for the introduction of a TZ above the passband (i.e. the phase shift of S-1-L is $+90° - 90° + 90° = +90°$ or $-90° - 90° - 90° = -270°$, whereas for S-L path is always $-90°$). Note that if direct couplings m_{s1} at each side of the resonator have the same sign, their coupling nature does not have any effect in the TZ position. Thus, electric or magnetic coupling mechanisms may be chosen for m_{s1} according to the specific characteristics of the coaxial SIW resonator, and not of the singlet itself.

Once the general position of the TZ with respect to the transmission pole is defined by choosing the sign of m_{sl}, its exact frequency position can be analytically computed as a function of the magnitude of m_{sl} as follows

$$\Omega_{TZ} = m_{s1}^2 / m_{sl} \tag{1}$$

where Ω_{TZ} is the normalized angular frequency. Hence, the frequency of the TZ can be determined by using the standard frequency transformation from low-pass to bandpass filter responses

$$\Omega = \frac{\Omega_C}{FBW}\left(\frac{\omega}{\omega_0} - \frac{\omega_0}{\omega}\right) \tag{2}$$

where $\Omega_C = 1$ rad/s, FBW and ω_0 are, respectively, the fractional bandwidth and centre angular frequency of the filter response, and ω is the real angular frequency.

A. COAXIAL SIW RESONATOR

In this work, the building block of the singlets is a microwave resonator implemented in coaxial SIW topology, following our recent approach described in [22]. The coaxial topology was recently proposed as a direct translation of the classical resonator of combline waveguide filters to a substrate integrated technology. This solution was proposed and extensively studied for implementing compact bandpass filters (BPFs) in several works, involving in-line direct couplings [25], [26] as well as cross-couplings [10], [27], [28] for implementing quasi-elliptic responses.

Coaxial SIW filters present important advantages in terms of compactness, and can easily accommodate magnetic and electric couplings in a single-layer structure, suitable for batch production using low-cost PCB fabrication procedures. Additionally, the structure can withstand moderate power levels, both in continuous and pulsed signal conditions, as proved in [26].

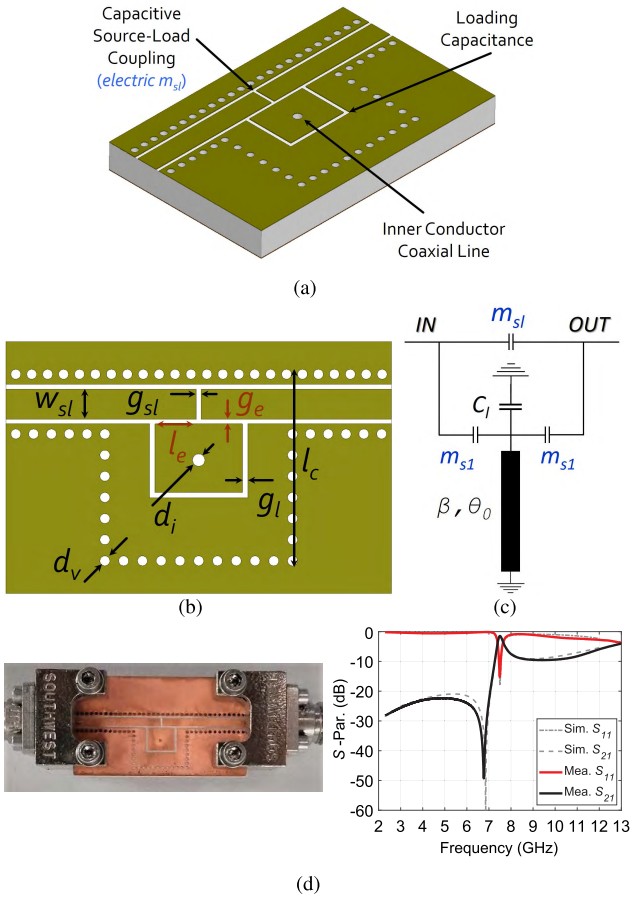

FIGURE 2. Coaxial SIW singlet with TZ below the passband demonstrated in [22]: (a) 3D view, (b) top view and (c) equivalent circuit. (d) Practical realization of a singlet in coaxial SIW topology with TZ below the passband, as we proposed in [22].

As Fig. 2 shows, in a coaxial SIW resonator, the inner post is short-circuited at the bottom metal layer and open-ended

at the top side. Thus, the resonator may be approximated as a piece of circular-square coaxial line of length h and characteristic admittance Y_0 embedded into the dielectric substrate [25]. The external square conductor is composed by the via hole walls that form the SIW cavity, while the coaxial inner circular conductor is the central plated post. The TEM-mode resonant frequency is given by the condition $B(\omega) = 0$, B being the susceptance of the coaxial resonator, which can be expressed as

$$B(\omega) = \omega C_l - \frac{1}{Z_0} \cot \beta h \tag{3}$$

where β is the TEM-mode propagation constant, C_l is the loading capacitance, and Z_0 is the coaxial line characteristic impedance.

In this context, the properties of a coaxial SIW resonator are defined by several parameters, thus increasing the design flexibility of such structures. Specifically, the laminate thickness h, the SIW cavity side l_c, the inner post diameter d_i, the perimeter and width g_l of the patch isolating gap (i.e. establishing C_l) allow us to fix the resonant frequency f_0 to its right value. These parameters are also set by adjusting the resonator slope parameter b, which basically defines the miniaturization degree of the resonator.

As it has been explained in [29], the susceptance slope parameter b for resonators having zero susceptance at ω_0 is defined as

$$b = \frac{\omega_0}{2} \frac{dB(\omega)}{d\omega}\bigg|_{\omega=\omega_0} \tag{4}$$

Hence, taking into account (3), the slope parameter for the proposed coaxial SIW topology can be particularised as follows

$$b = \frac{1}{2}\left[\omega_0 C_l + \frac{\theta_0}{Z_0 \sin^2 \theta_0}\right]. \tag{5}$$

where θ_0 is the resonator electrical length at the desired resonant frequency f_0 (i.e. $\theta_0 = \beta_0 h$).

B. SINGLET WITH TZ ABOVE THE PASSBAND

Fig. 2 depicts the layout of the coaxial SIW singlet with a TZ below the passband that was recently reported in [22]. The equivalent circuit of the proposed SIW singlet is depicted in Fig. 2-(c). The latter reflects the fact that an electric coupling scheme enables a flexible direct source/load coupling m_{sl} (see Fig. 2-(b)) that bypasses the resonating mode and generates a singlet response. In this context, Fig. 2-(d) shows the practical implementation of such coaxial SIW singlet and its measured results [22], whose agreement with 3D EM simulation is remarkable.

Such bypass is easily implemented by means of an additional distributed capacitance that is created on the CPW feeding line. As well known, the fundamental TEM mode of coaxial SIW resonators can be excited by means of an electric coupling mechanism based on a distributed capacitance [10], [28], embedded into the dielectric.

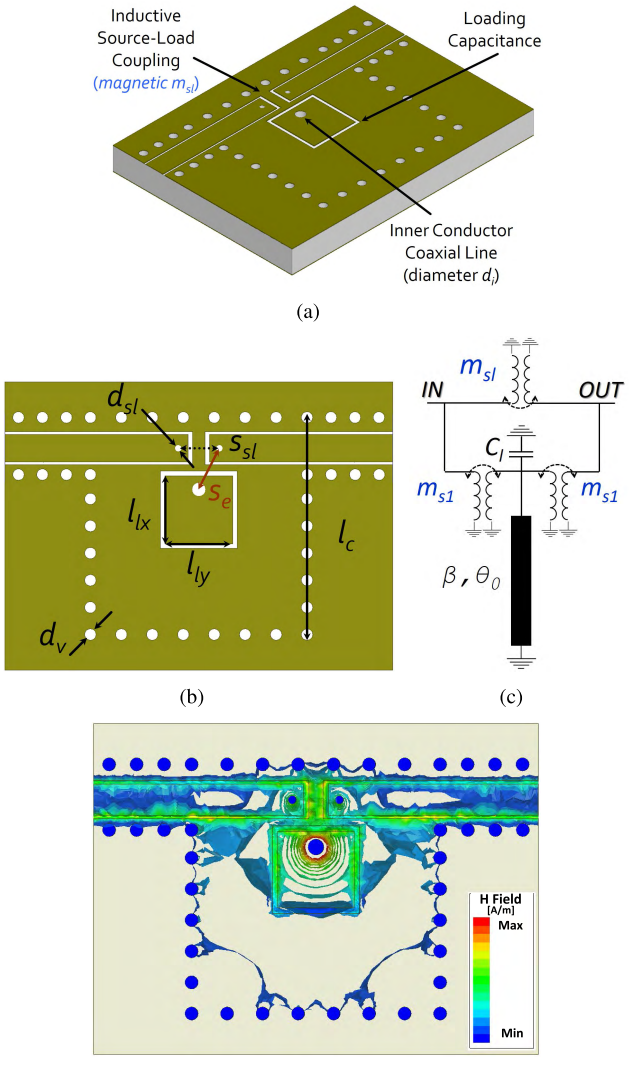

FIGURE 3. Coaxial SIW singlet with TZ above the passband: (a) 3D view, (b) top view, (c) equivalent circuit, and (d) magnetic field patterns of the TEM mode and feeding ports. Sizes: $w_{sl} = 1.2$ mm, $s_{sl} = 1.8$ mm, $s_e = 2$ mm, $l_{lx} = l_{ly} = 3$ mm, $d_i = 0.6$ mm, $d_{sl} = 0.3$ mm and $d_v = 0.5$ mm.

Fig. 2-(b) shows that the capacitance associated to m_{sl} is controlled by the spacing g_{sl} and width w_{sl}. It is remarkable that a single layer PCB fabrication is still suitable for implementing such topology, thus reducing cost and complexity of the solution.

As previously explained, if the m_{sl} is based on a magnetic coupling mechanism, the TZ of the singlet appears above the transmission pole. To provide such a magnetic coupling in coaxial SIW topology, a standard CPW-to-SIW transition that makes use of a current probe is employed, as shown in Fig. 3. This excitation mechanism, whose first demonstration was provided in [30], has been recently proposed as an effective mechanism for the external coupling of evanescent mode SIW filters [14], [28].

Therefore, a plated via hole having diameter d_{sl} is now inserted at the end of the CPW feeding lines, and is then

short-circuited to the bottom ground plane. The plated via hole can be seen as an extension of the CPW feeding line, which should be terminated by an open circuit immediately following the plated via hole. As proved in [30], the current flowing through the plated via hole generates a magnetic field that excites the fundamental mode of the resonator, which is, in our case, the TEM mode of the coaxial SIW cavity. Taking into account that the TEM mode shows a high current that flows through the inner via hole having diameter d_i, this mechanism provides an effective way to excite the coaxial SIW fundamental mode, as it is clearly visible in Fig. 3-(d).

It is worth mentioning that in order to obtain such magnetic coupling feature by using the proposed mechanism, it is crucial to ensure ground planes among both the spacing gaps of input and output CPW feeding lines, and between those lines and the loading capacitance, as depicted in Fig. 3-(b). By doing that, it is possible to avoid fringing fields among these isolated conductors, thus eliminating the electric coupling component and enhancing the total coupling.

Indeed, as proposed in [28], when these current probe holes inserted at the end of the feeding lines are faced each other with the only separation of an air gap, a mixed coupling mechanism is generated. The magnetic component relies mostly on the separation of the plated holes, whereas the electric component depends on the width of the air gap between feeding line conductors. Since these two couplings are out of phase, the total coupling can be extracted as the magnetic coupling minus the electric coupling. Such property was exploited in [28] to produce an external coupling cancellation at specific frequencies, which allows us to generate additional TZs in the frequency response of coaxial SIW filters.

Finally, the great advantage of this solution is the simple introduction of a magnetic bypass coupling between source and load by approaching the input and output feeding lines to each other, and especially their coupling posts. Furthermore, this solution is perfectly compatible with low-cost single-side PCB fabrication processes, whereas it maintains the high miniaturization degree of the coaxial topology. In fact, such coaxial SIW resonator configuration provides more than 45% of resonant frequency reduction with respect to a standard TE_{101} SIW cavity resonator, being comparable to the size of a half-mode SIW implementation, but showing a higher Q_u.

1) DESIGN

Let us consider a singlet whose frequency response shows a transmission pole at 7.5 GHz, in-band return loss (RL) of 15 dB, whereas the FBW_{3dB} has been set to 4.5%, as shown in Fig. 4. Specifically, the resonator slope parameter b has been set to 24.5 mS, thus the resonator parameters are: coaxial characteristic impedance $Z_0 = 91\,\Omega$, resonator electrical length $\theta_0 = 26°$ at 7.5 GHz, and capacitive patch $C_l = 480\,\text{fF}$ (i.e. $l_{lx} = l_{ly} = 3\,\text{mm}$ with $g_l = 0.2\,\text{mm}$). In addition, let us consider the use of a 1.52 mm-thick Rogers R04003C laminate with permittivity $\epsilon_r = 3.55$ as dielectric substrate.

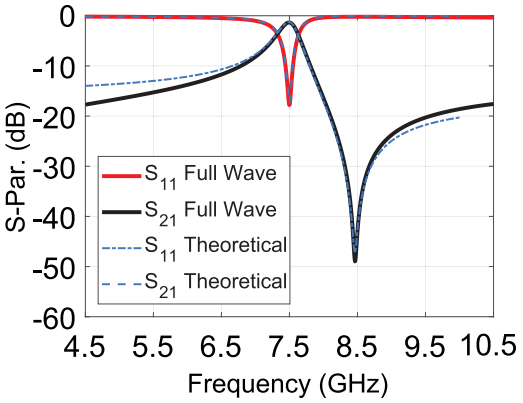

FIGURE 4. Theoretical (*dashed lines*) and simulated (*solid lines*) responses of the coaxial SIW singlet of Fig 3.

By setting the inner via diameter at $d_i = 0.6\,\text{mm}$, the SIW cavity size becomes $l_c = 10 \times 10\,\text{mm}^2$. It is worth mentioning that this coaxial SIW configuration is able to reduce f_0 of about 36% if compared to a standard TE_{101} approach (i.e. from 11.8 GHz to 7.5 GHz).

By using the magnetic m_{sl}, the TZ is generated above the passband, at 8.5 GHz. Fig. 4 shows the theoretical and simulated responses of this singlet, whose coupling matrix elements are: $m_{s1} = 0.66$, $m_{sl} = 0.083$, and $m_{11} = 0$.

Basically, the TZ position is defined by two distinct parameters, which are the coupling post diameter d_{sl} and the separation s_{sl} between the coupling posts of the input and output feeding lines (see Fig. 3-(b)). Indeed, Fig. 5 shows how the TZ may be finely set by adjusting d_{sl} (see Fig. 5-(a)) or s_{sl} (see Fig. 5-(b)). In the latter case, separating the coupling posts from 1.55 mm to 2.05 mm, the TZ location may be set in a frequency range of about 600 MHz, from 8.2 GHz to 8.8 GHz.

Furthermore, the separation s_e among the CPW coupling posts and the center post of the coaxial SIW defines the magnitude of m_{s1}. The energy coupled into the coaxial SIW resonator increases for smaller s_e, as it is visible in Fig. 6, thus achieving higher m_{s1}.

However, due to the working principle and layout geometry of this magnetic coupling, the values of m_{sl} and m_{s1} have a slight mutual dependence. On one hand, the distances s_e and s_{sl} are both dependent variables of the positions of the same via holes. On the other hand, as for the m_{sl}, the energy transfer from the CPW coupling post to the center post relies upon the via hole diameters, which are d_i and d_{sl}. This means that the design of a magnetic-based singlet is more time consuming than that of the electric-based singlet demonstrated in [22].

III. CASCADED SINGLETS IN COAXIAL SIW

A key feature of using singlets for designing bandpass filters is the extremely high modularity of this solution. By cascading N singlets, the design of elliptic filters of order N having N TZs in the frequency response is enabled, showing also the remarkable ability of each singlet to independently control its own TZ.

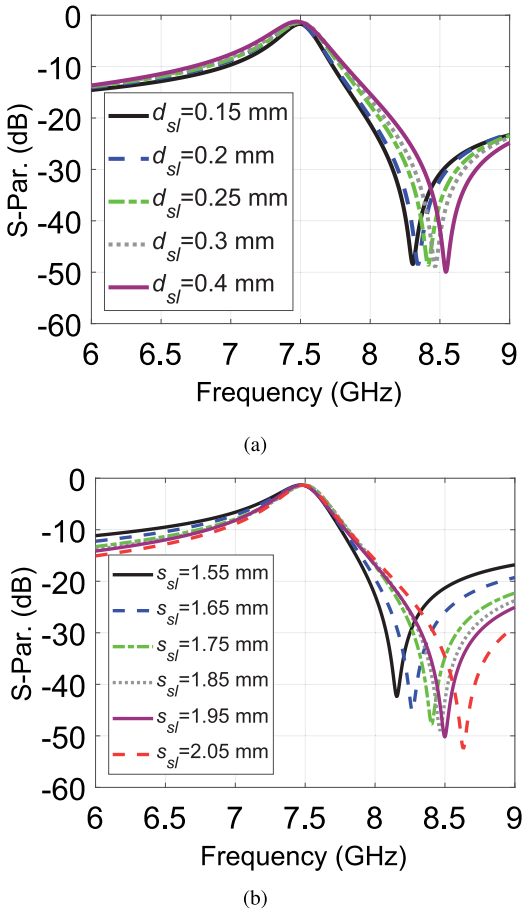

FIGURE 5. S_{21}-parameter response of the coaxial SIW singlet with magnetic m_{sl} when (a) the coupling via hole diameter d_{sl}, and (b) the coupling holes spacing s_{sl} are changed.

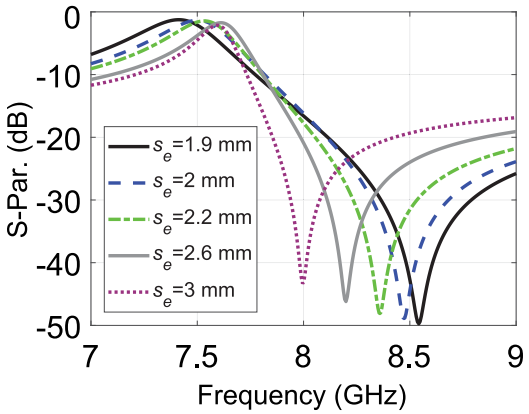

FIGURE 6. S_{21}-parameter responses of the coaxial SIW singlet with magnetic source/load coupling when varying s_e.

In order to validate the performance of the proposed singlet concept, the next three examples of advanced filtering responses, based on the guidelines from Section II, are considered:

- A two-pole BPF having two TZs above the passband in Section III-A.
- A two-pole BPF with two TZs at both sides of the passband in Section III-B.
- The latter example in Section III-C is a third order BPF with three TZs, two of them below and one above the passband.

It is worth mentioning that to cascade adjacent singlets, a NRN is used as coupling mechanism. In this work, a quarter-wave CPW section created at the top metal layer, and embedded into the resonators, is used as NRN. The NRN layout is shown in Fig. 7-(b), which highlights that the main parameters of such piece of CPW line are its length l_{nrn}, its width w_{nrn} and the spacing gap g_{nrn}.

The substrate laminate that has been chosen for implementing the three proposed designs is again Rogers R04003C substrate ($\epsilon_r = 3.55 \pm 0.05$, $\tan\delta = 0.0027$ at 10 GHz) having thickness of 1.52 mm. All 3D EM simulations that will be shown in the following sections have been obtained by using Ansys HFSS.

A. CASCADED SINGLETS WITH TWO TRANSMISSION ZEROS ABOVE THE PASSBAND

In the first example, a narrow-band BPF centered at $f_c = 7.5$ GHz with a fractional bandwidth $\text{FBW}_{1\text{dB}} = 4.6\%$ (i.e. BW = 340 MHz) and RL = 15 dB is designed, fabricated and measured. By cascading two coaxial SIW singlets featuring magnetic m_{sl}, the rejection of the second-order BPF can be strongly improved above the passband thanks to the introduction of two TZs. The filter routing scheme is shown in Fig. 7-(a), where numbered grey circles are coaxial SIW resonator nodes, patterned circles indicating $(N1, N2)$ are non-resonating nodes, whereas S, L are source and load port, respectively. Furthermore, m_{si} are main direct couplings, and $m_{sl,i}$ are cross couplings. Finally, the values of filter coupling matrix elements are shown in Table 1.

TABLE 1. Coupling matrix of the designed two cascaded singlets.

m_{s1}	0.94	m_{s2}	0.75
$s_{sl,1}$	0.082	$m_{sl,2}$	0.103
m_{11}	0.21	m_{22}	-0.12
$m_{n1,n2}$	0.81		

Fig. 7-(b) shows the filter layout. Since the TZs will appear above f_c in this configuration, the self-resonance of the NRN f_{nrn} is now designed to be much lower than f_c. Thus, the NRN length has been increased up to 13.4 mm, so that f_{nrn} is now centered at 5 GHz. In this context, Table 2 shows the main sizes of the designed two-pole filter.

The separation among coupling posts s_{sl1} and s_{sl2} independently control, respectively, the position of each TZ. In this design, these are generated at $f_c + 3 \times \text{BW} = 8.5$ GHz, and $f_c + 6 \times \text{BW} = 9.5$ GHz. Hence, the filter would provide a rejection better than 40 dB from 8.2 GHz up to 10.2 GHz.

Finally, the SIW cavity side is $l_c = 9.8 \times 9.8\,\text{mm}^2$, and the inner d_i is set to 0.6 mm. The resonators show the same characteristics of the singlet of Section II-B, whose

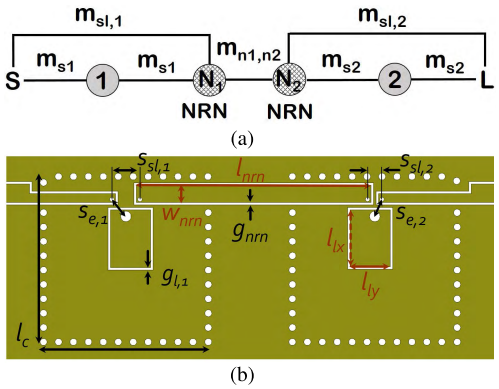

FIGURE 7. (a) Routing scheme and (b) layout of the two cascaded singlets with a quarter-wave CPW NRN that introduces two TZs above the passband.

TABLE 2. Layout dimensions of the designed two cascaded singlets (Unit: mm).

$s_{sl,1}$	1.6	$s_{sl,2}$	0.83
$s_{e,1}$	1.26	$s_{e,2}$	1.05
$l_{lx,1}$	3.3	$l_{lx,2}$	3.26
$l_{ly,1}$	2.3	$l_{ly,2}$	2.3
$g_{l,1}$	0.14	$g_{l,2}$	0.14
l_c	9.8	g_{nrn}	0.15
l_{nrn}	13.4	w_{nrn}	0.98
d_v	0.4	d_i	0.6

parameters are: $b = 24.5$ mS, $Z_0 = 90\ \Omega$, $\theta_0 = 25.9°$, and $C_l = 480$ fF. However, the final size excluding the feeding lines of the cascaded singlets has been widened by the longer NRN, being $9.8 \times 24\,\text{mm}^2$ that corresponds to $0.25 \times 0.6\lambda_0^2$ and $0.46 \times 1.13\lambda_g^2$, where λ_g is the guided wavelength at 7.5 GHz.

1) MEASUREMENTS

This prototype with cascaded singlets has been fabricated in a single-layer PCB process by using an etching fabrication process (i.e. based on a photo-imageable film application followed by a photo-exposure) with electroless nickel immersion gold (ENIG) finishing. Such process shall allow us to implement lines and isolating gaps with a width of less than 0.2 mm.

Lossless theoretical and simulated responses are shown in Fig. 8-(a). The measurements of the fabricated device are shown in Fig. 8-(b), where the initial and back-simulations are included, whereas a photograph of the filter prototype is visible in Fig. 8-(c). Indeed, the filter response has suffered a frequency shift from 7.5 GHz to 7.7 GHz (i.e. +2.7%) due to the non-vertical edges of the capacitive patch gaps, and the reduced final finishing thickness. By using a stylus profilometer, the latter has been measured to be around 30 μm instead of the expected value of 50 μm. Such deviations of the component sizes have been included in the 3D model, and additional EM simulations (i.e. a back-simulation approach)

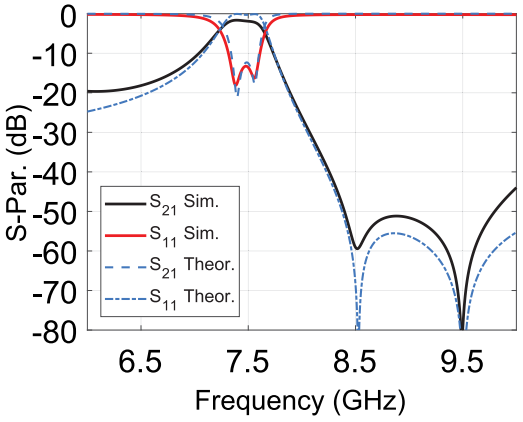

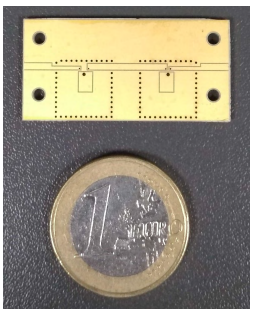

FIGURE 8. Two-pole cascaded singlets filter of Fig 7: (a) lossless theoretical response (*dashed lines*) and simulations (*solid lines*), (b) simulations (*dotted line*), measurements (*solid lines*) and back-simulations (*dashed lines*) that fit the measurements. (c) Photograph of a fabricated filter prototype.

have been performed and shown in Fig. 8-(c). As it can be clearly observed, both deviations affect the final value of C_l, which is slightly lower than the nominal design value, thus justifying the frequency shift to higher frequencies that has been measured.

Apart from the frequency shift, the filter response is in good agreement with simulation results. The measured IL and RL are, respectively, 2.2 dB and 21 dB, which are similar to the simulated values of IL = 1.9 dB and RL = 15 dB.

From measurements, the extracted Q_u of the singlets is around 150. The TZs are located 1 GHz and 2 GHz above the filter f_c (i.e. at 8.7 GHz and 9.7 GHz), providing more than 40 dB of rejection between 8.5 GHz and 10.5 GHz, which are values comparable to the desired ones.

B. CASCADED SINGLETS WITH TWO TRANSMISSION ZEROS AT BOTH SIDES OF THE PASSBAND

Combining the singlet with magnetic m_{sl} described in Section II-B and the singlet with electric m_{sl} already described in [22], it is possible to exploit the modularity of such approach. This enables us to design a two-pole filter with TZs located at both sides of the passband, whose routing scheme is shown in Fig. 9-(a).

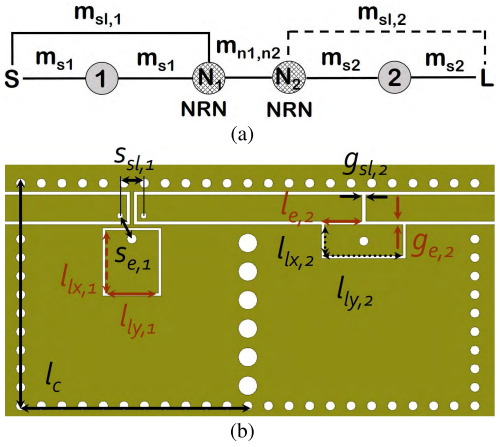

FIGURE 9. (a) Routing scheme and (b) layout of the two cascaded singlets with a quarter-wave CPW NRN that introduces two TZs at both sides of the passband.

The layout of the proposed device is shown in Fig. 9, whereas its main dimensions are listed in Table 3. As for the cascaded singlets of Section III-A, to implement such filtering response the two singlets are cascaded by means of the quarter-wave CPW NRN structure.

TABLE 3. Layout dimensions of the designed two cascaded singlets with TZs at both passband sides (Unit: mm).

$w_{sl,1}$	1.1	$s_{e,1}$	1.15
$s_{sl,1}$	1	$d_{sl,1}$	0.25
$l_{lx,1}$	2.63	$l_{ly,1}$	2.25
$g_{sl,2}$	0.175	$g_{e,2}$	0.15
$l_{e,2}$	1.57	$w_{sl,2}$	1.1
$l_{lx,2}$	1.3	$l_{ly,2}$	3.31
$g_{l,1}$	0.125	$g_{l,2}$	0.125
$l_{c,x}$	9.8	$l_{c,y}$	10
$d_{i,1}$	0.4	$d_{i,2}$	0.4
d_v	0.4	g_{nrn}	0.15
l_{nrn}	9.5	w_{nrn}	1.1

Specifically, the proposed BPF with TZs at both sides of the passband has been designed to be centered at the very same frequency of the previous devices, which is $f_c = 7.5$ GHz, having $\text{FBW}_{3\text{dB}} = 5\%$ (i.e., which means that the filter BW $= 375$ MHz) and RL $= 15$ dB. It is worth mentioning that the NRN has been optimized to show a resonant frequency below 4 GHz, thus far below f_c. The coupling matrix elements of such desired frequency response are shown in Table 4.

TABLE 4. Coupling matrix of the designed two cascaded singlets with TZs at both passband sides.

m_{s1}	0.766	m_{s2}	-0.94
$s_{sl,1}$	0.083	$m_{sl,2}$	-0.125
m_{11}	0.42	m_{22}	-0.21
$m_{n1,n2}$	0.79		

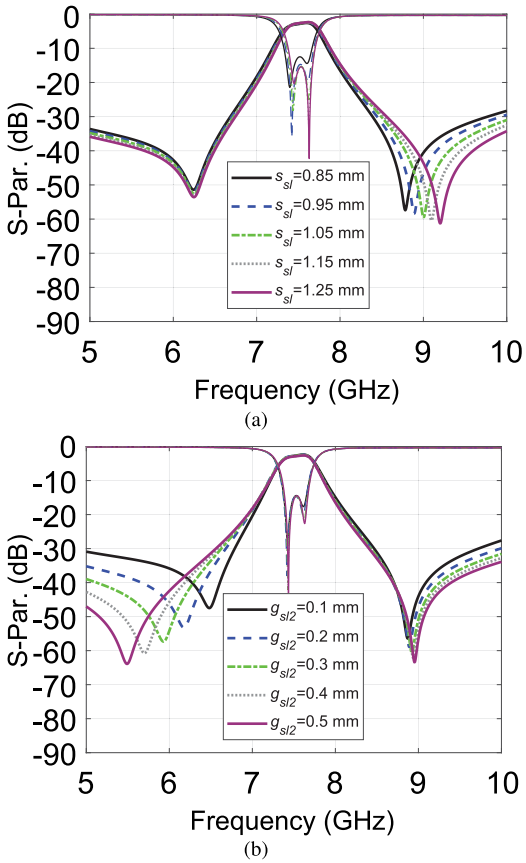

FIGURE 10. Cascaded singlets with two TZs at both sides of passband: (a) upper TZ position can be controlled by adjusting $s_{sl,1}$, and (b) lower TZ position is modified by using $g_{sl,2}$.

Fig. 10-(a) and (b) demonstrate how the position of both TZs can be controlled independently by adjusting the related bypass coupling magnitude. As for the singlets previously described, the distance $s_{sl,1}$ is setting the TZ that is generated above the passband (see Fig. 10-(a)), whereas the position of the lower TZ is controlled by $g_{sl,2}$ (see Fig. 10-(b)). It is worth noting that the filter RL slightly changes when the magnetic bypass coupling is modified, as it has been explained in Section II-B. Finally, $m_{sl,1}$ and $m_{sl,2}$ have been set to generate the lower TZ at $f_c - 3.5 \times \text{BW} = 6.2$ GHz, and the upper TZ at $f_c + 4 \times \text{BW} = 9$ GHz.

1) MEASUREMENTS

Theoretical and simulated responses of this BPF are shown in Fig. 11-(a). On the other hand, a comparison between simulations, measurements and back-simulations are shown in Fig. 11-(b), whereas Fig. 11-(c) depicts a photograph of the manufactured filter prototype.

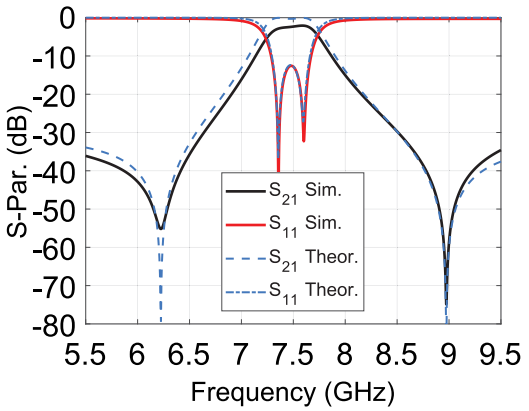

(a)

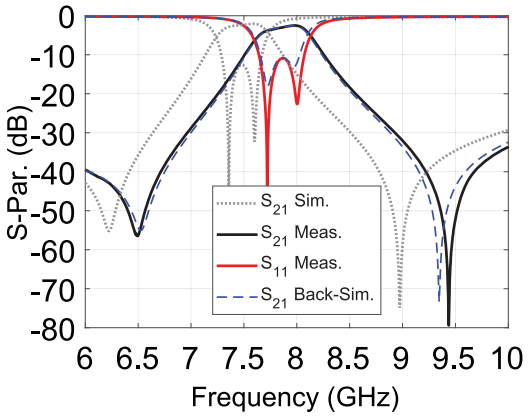

(b)

(c)

FIGURE 11. Two-pole cascaded singlets with two TZs at both sides of passband of Fig 9: (a) lossless theoretical responses (*dashed lines*) and simulations (*solid lines*), (b) simulations (*dotted line*), measurements (*solid lines*) and back-simulations (*dashed lines*) that fit the measurements. (c) Photograph of a fabricated filter prototype.

Since this filter prototype has been fabricated in the same manufacturing batch of the BPF presented in Section III-A, the aforementioned manufacturing problems are also affecting the response of this filter. Indeed, in this case the filter response has been shifted from 7.5 GHz to 7.85 GHz (i.e. +4.7%).

The measured IL and RL are in good agreement with the simulated values. On one hand, the measured RL is 12 dB, instead of being 15 dB. On the other hand, the measured in-band IL varies from 2.5 dB at the upper cutoff frequency of passband to 3.8 dB at the lower one, whereas, in simulations, this IL variation should be from 2 dB to 2.8 dB. The in-band flatness is more than 1 dB, due to the unequal Q_u of the resonators which have different configurations. Specifically, from measurements, the Q_u of the first singlet has been estimated to be close to 150, whereas the Q_u of the second one is approximately 100.

Despite the frequency shift, the positions of the TZs show a high concordance among back-simulations and measurements, thus confirming the flexibility of the proposed solution.

C. THREE CASCADED SINGLETS WITH THREE TZS

In the last example of BPF based on cascaded singlets, the design modularity is proved by designing a third-order elliptic filter with two TZs below, and one TZ above the passband. This filtering response can be implemented by cascading three singlets with different source-load coupling mechanisms. The filter centre frequency is again $f_c = 7.5$ GHz whereas the FBW measured at the level of RL $=$ 15 dB is 5% (i.e. BW $= 380$ MHz). The singlets are coupled among them by means of the quarter-wave CPW NRNs, whose resonant frequencies are much lower than the filter f_c. For instance, in this design, NRNs resonate around $f_{nrn} \simeq 4$ GHz, as it can be seen in Fig. 13-(a). In this context, the coupling matrix elements of the frequency response can be seen in Table 5.

TABLE 5. Coupling matrix of the designed three cascaded singlets.

m_{s1}	-0.96	m_{s2}	0.64	m_{s3}	-0.76
$s_{sl,1}$	-0.175	$m_{sl,2}$	0.11	$m_{sl,3}$	-0.046
m_{11}	-0.33	m_{22}	0.39	m_{33}	0.04
$m_{n1,n2}$	0.83	$m_{n2,n3}$	0.6		

Fig. 12-(a) shows the three cascaded singlets layout, while in Fig. 12-(b) the theoretical and simulated results are compared. The main dimensions of this filter are shown in Table 6, where p_d is the pitch between adjacent holes forming the cavity sides.

It is worth mentioning that the overall BPF size is 9.8×28.5 mm^2 (i.e. $0.25 \times 0.71\lambda_0^2$ and $0.46 \times 1.34\lambda_g^2$, where λ_g is the guided wavelength at 7.5 GHz) excluding the feeding lines, which exhibits an important degree of miniaturization with respect to standard SIW approaches. Two singlets having electric cross-coupling have been used as first and third resonator to generate two TZs below the passband. More specifically, the farthest TZ is located at

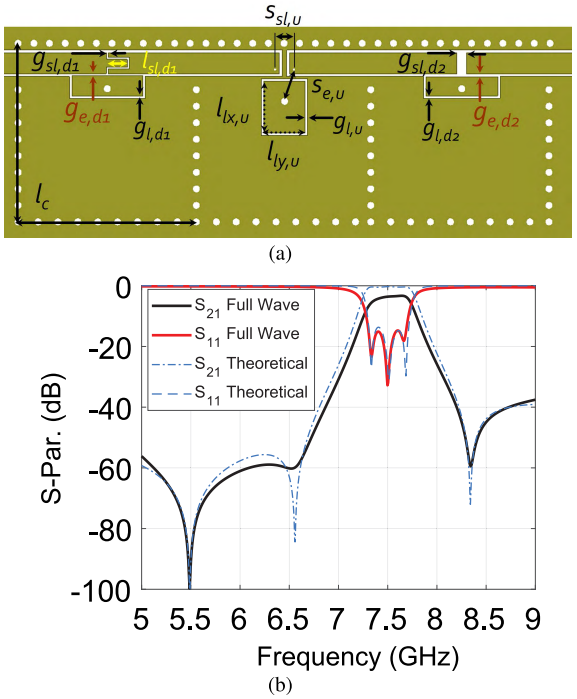

FIGURE 12. Three-pole elliptic BPF based on three cascaded singlets: (a) layout, and (b) lossless theoretical and simulated responses.

TABLE 6. Layout dimensions of the designed three cascaded singlets (Unit: mm).

$g_{e,d1}$	0.135	$g_{sl,d1}$	0.125	$l_{sl,d1}$	1.12
$l_{lx,d1}$	1	$g_{l,d1}$	0.15	$l_{ly,d1}$	3.95
$s_{sl,u}$	1.1	$d_{sl,u}$	0.25	$s_{e,u}$	1.85
$g_{l,u}$	0.145	$l_{lx,u}$	2.7	$l_{ly,u}$	2.3
$g_{sl,d2}$	0.5	$g_{e,d2}$	0.165	$g_{l,d2}$	0.145
$l_{lx,d2}$	1	$l_{ly,d2}$	3.79	l_c	9.8
$d_{i,1}$	0.4	$d_{i,2}$	0.4	$d_{i,3}$	0.4
$l_{nrn,1}$	9.05	$l_{nrn,2}$	8.85	w_{nrn}	1.1
d_v	0.4	w_{sl}	1.1	p_d	0.9

5.5 GHz, thus 2 GHz below f_c, and the other one is centered at $f_c - 2.5 \times \text{BW} = 6.55$ GHz. On the other hand, one TZ is generated above the filter passband by the second cascaded singlet, which has a magnetic m_{sl}. This upper TZ has been set at $f_c + 2.25 \times \text{BW} = 8.35$ GHz. It is remarkable that three TZs have been introduced in a standard in-line filter topology without the use of any cross-coupling between non-adjacent resonators.

1) MEASUREMENTS

For verifying the proposed filter configuration, a prototype of the quasi-elliptic BPF of Fig. 12-(a) has been implemented using again a 1.52 mm-thick Rogers R04003C ($\epsilon_r = 3.55$, $\tan\delta = 0.0027$ @ 10 GHz), and fabricated in single-layer PCB process. A photograph of the fabricated filter is shown in Fig. 13, together with its simulated and measured responses that give us an indication of the good agreement between them, even if a frequency shift of the measured response is

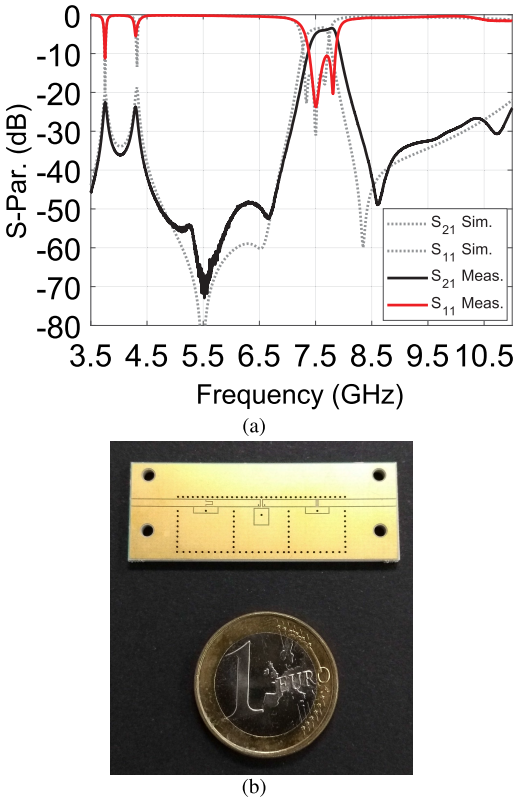

FIGURE 13. Three-pole elliptic BPF based on three cascaded singlets: (a) a comparison between measured and simulated responses, and (b) a photograph of the filter prototype.

again visible. Specifically, the aforementioned manufacturing problems are also affecting the response of this filter, resulting in a shift of the passband center from 7.5 GHz to 7.67 GHz (i.e. +2.2%).

The measured RL is now 11 dB at 7.7 GHz, which is slightly worse than desired, whereas the filter FBW keeps the designed value. Furthermore, the measured in-band IL varies from 3.5 dB at the upper cutoff frequency of the passband to 4.5 dB at the lower one, which means that there is a very good agreement between simulations and measurements. For instance, at these specific frequencies, the IL has been estimated to vary from 3.3 dB to 4.2 dB including the ENIG finishing for the metal layers in the 3D model. Therefore, the in-band flatness is around 1 dB in both case, which is mainly due to the unequal Q_u of the distinct coaxial SIW resonators. From measurements, the Q_u of the first and third singlets with electric m_{sl} are estimated to be close to 100, whereas the Q_u of the second singlet having magnetic m_{sl} is approximately 150.

A further analysis of the results of Fig. 13-(a) shows that the rejection is better than 48 dB between 4.5 GHz and 6.7 GHz, and it is better than 25 dB above the passband, from 8.2 GHz to 11 GHz, showing excellent concordance with simulations. Above, as expected, the rejection worsens due to the first spurious mode of the SIW cavity that resonates at 12.5 GHz.

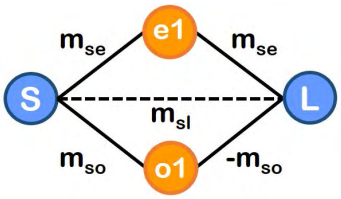

FIGURE 14. Routing scheme of the doublet with source-load electric coupling proposed in [22].

IV. DOUBLETS AND DUAL-BAND FILTERS BASED ON DUAL-MODE COAXIAL SIW

In this section, the design of flexible dual-band filters based on a doublet filtering topology with bypass coupling are introduced, and demonstrated with the implementation and characterization of two prototypes.

As it is well known, a doublet presents two separate coupling paths between the source and the load that allow the generation of one TZ, whose position depends on the coupling coefficients and their relative signs [23]. In [22], a fully integrated technique for generating an additional TZ in such topology was successfully proved by using a direct source-load path. Specifically, the direct source-load m_{sl} coupling, which is based on an embedded electric coupling mechanism, enables the fine control of the position of the additional TZ. Therefore, such doublet topology, whose routing coupling path is shown in Fig. 14, allows for the design of extremely compact quasi-elliptic filtering responses. Note that, in Fig. 14, $e1$ and $o1$ indicate the even- and odd-mode resonator node, respectively, whereas m_{se} and m_{so} are the main direct couplings to the even- and odd-mode, respectively.

Such promising approach is now applied to the design of dual-band filters that feature two independently controllable bandwidths in just one single SIW cavity resonator, thus further enhancing the frequency-selectivity and the miniaturization degree provided by the dual-mode coaxial SIW topology, firstly proposed in [23] and [31].

A. DUAL-BAND FILTERS BASED ON DOUBLETS

As a further demonstration of the design flexibility offered by the proposed doublet configuration with direct bypass coupling, two dual-band filters with TZs at both sides of the passbands, and with different bandwidth requirements, are designed, fabricated and measured. Figs. 15 and 16 show the layouts of the proposed dual-band filters, which are named in the following as filter DB1 (see Fig. 15) and filter DB2 (see Fig. 16), whereas the main dimensions of these devices are listed in Table 7.

In those layouts, two different dual-mode coaxial SIW resonators have been inserted into the same SIW cavity, each one providing a different passband. For that, two pairs of plated via holes are symmetrically inserted with respect to the transverse side of the cavity, and at each side of the CPW feeding line, which is symmetrically placed along the longitudinal side of the SIW cavity.

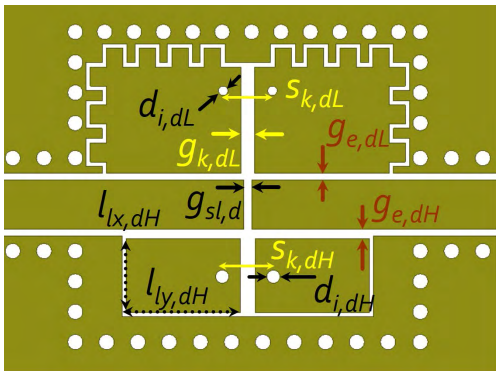

FIGURE 15. Layout of the dual-band filter DB1.

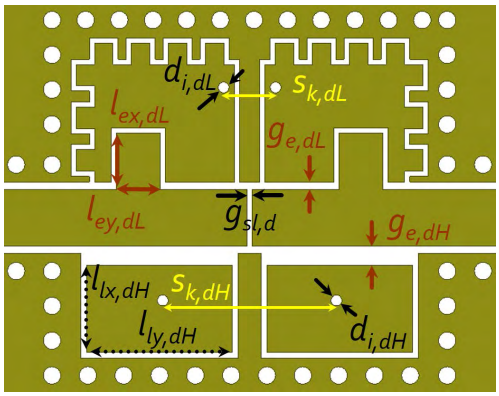

FIGURE 16. Layout of the dual-band filter DB2.

TABLE 7. Layout dimensions of the designed filters DB1 and DB2 (Unit: mm).

Size	DB1	DB2	Size	DB1	DB2
w_{s1}	1.3	1.3	$g_{sl,d}$	0.2	0.12
$s_{k,dL}$	1.3	1.2	$s_{k,dH}$	1.35	4
$g_{e,dL}$	0.175	0.12	$g_{e,dH}$	0.245	0.45
$l_{lx,dH}$	1.95	2	$l_{ly,dH}$	3	3.35
$g_{l,dL}$	0.115	0.12	$g_{l,dH}$	0.115	0.12
$l_{cx,d}$	8.1	8.1	$l_{cy,d}$	9.2	9.2
$d_{i,dL}$	0.25	0.25	$d_{i,dH}$	0.35	0.25
d_v	0.4	0.4	w_{sl}	1.25	1.25

This configuration can be perfectly modeled by means of the coupling diagram of Fig. 17. From this model, it can be deduced that both passbands can be independently controlled, since there is no coupling between the upper and lower side of the cavity (i.e., between each dual-mode resonator), which is a very interesting property. Another important feature is that this topology is able to provide up to four TZs placed at real frequencies, which can be used for the design of dual-band filters with very selective responses and high rejection levels between bands, as will be shown next.

The proposed dual-band topology enables us to use the electric coupling mechanism to implement completely independent external couplings for each dual-mode resonator. As Figs. 15 and 16 show, the spacing gaps $g_{e,dL}$ and $g_{e,dH}$ set,

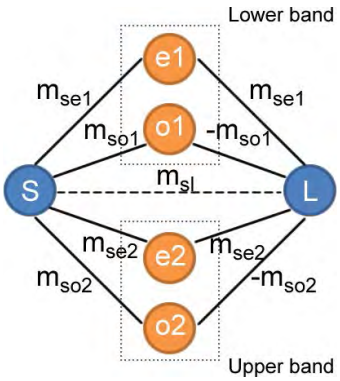

FIGURE 17. Routing coupling scheme of the proposed dual-band filter topology.

separately, the values of the embedded coupling capacitances that control the external coupling of each band. In addition, an inter-digital capacitor topology gives a straightforward approach for increasing the external coupling if required, as well as for boosting C_l of a coaxial SIW resonator, following the approach proposed in [32]. To increase the external coupling in the lower band of the filter DB2, as it is shown in Fig. 16, two insets are created, and are defined by the sizes $l_{ex,dL}$ and $l_{ey,dL}$, as well as by the gap $g_{e,dL}$. By increasing $l_{ex,dL}$ the external coupling can be easily increased.

Furthermore, square-shaped inter-digital capacitors are introduced in both lower bands of the filter DB1 and DB2, as it is visible in Figs. 15 and 16, to provide a highly loaded coaxial SIW configuration that allows for a strong reduction of the center frequency of these bands. Indeed, both dual-band filters have a size of $l_{c,d}^2 = 8.1 \times 9.2\,\text{mm}^2$ (i.e. $0.14 \times 0.16\lambda_0^2$ and $0.26 \times 0.3\lambda_g^2$, where λ_g is the guided wavelength at 5.25 GHz), which implies a remarkable degree of miniaturization. It is, therefore, clear that the proposed approach is able to maximize the miniaturization of bandpass filters based on the coaxial SIW topology. Finally, the passband bandwidths are easily set by adjusting the TEM even and odd modes frequencies of each pair, which can be done by modifying the via hole separation $[s_{k,dL}, s_{k,dH}]$ and the spacing gaps $[g_{k,dL}, g_{k,dH}]$.

In order to prove the design flexibility and the high degree of independence between bands during the design step, two dual-band filters with very different passband requirements are designed. On one hand, the dual-band filter DB1 is operating at 5.3 GHz and 7.85 GHz providing $\text{FBW}_{1\text{dB}} = 8.2\%$ (i.e. BW = 435 MHz) and $\text{FBW}_{1\text{dB}} = 11\%$ (i.e. BW = 870 MHz), respectively.

On the other hand, the filter DB2 operates at 5.25 GHz and 7.5 GHz, providing $\text{FBW}_{1\text{dB}} = 12.8\%$ (i.e. BW = 670 MHz) and $\text{FBW}_{1\text{dB}} = 2.7\%$ (i.e. BW = 200 MHz), respectively. Note that the frequency ratios of the second band to the first band are 1.48 and 1.42, respectively, for the filter DB1 and DB2.

The coupling matrix elements for these filters are listed in Table 8. These values are computed for $f_c = 7$ GHz (intermediate frequency between bands) and FBW = 50% (this bandwidth covers the two passbands for both filters).

TABLE 8. Coupling matrix of the filters DB1 and DB2.

Coupling element	Filter DB1	Filter DB2
m_{se1}	0.2425	0.304
m_{so1}	0.2462	0.3172
m_{se2}	0.2677	0.1542
m_{so2}	0.2779	0.1375
m_{ee1}	1.3211	1.4921
m_{ee2}	0.9591	0.9442
m_{oo1}	-0.2224	-0.217
m_{oo2}	-0.6405	-0.3293
m_{sl}	-0.12	-0.105

Concerning the bypass coupling dimensions, in the filter DB1, the spacing $g_{sl,d}$ is set to 0.2 mm, while it is 0.12 mm in the filter DB2, thus, TZs are introduced with different separations to the passbands. It is worth mentioning that the position of TZs due to the dual-mode configuration is slightly affected by the magnitude of the bypass coupling m_{sl}. This means that a few iterations may be needed to optimize the design by using simulations.

1) MEASUREMENTS

Simulations, measurements, and back-simulations of the prototypes of the filters DB1 and DB2 are shown, respectively, in Fig. 18-(a) and Fig. 18-(b), and a photograph of the devices is depicted in Fig. 18-(c). A comparison between the simulated and measured results of the doublet prototypes is listed in Table 9. Since the two dual-band filter prototypes belong to the same manufacturing batch of the previous cascaded singlets, a systematic frequency shift appears among simulated and measured responses of both devices.

TABLE 9. Comparison between initial simulations and measurements for the filters DB1 and DB2 (Note: L = lower band, U = upper band, TZ_1 = lower TZ expressed as f_{tz1}/f_{cL} and f_{tz1}/f_{cU}, and TZ_2 = upper TZ expressed as f_{tz2}/f_{cL} and f_{tz2}/f_{cU}).

	Sim. DB1 (L / U)	Meas. DB1 (L / U)	Sim. DB2 (L / U)	Meas. DB2 (L / U)
f_{cL}/f_{cU} (GHz)	5.3 / 7.85	5.65 / 8.4	5.25 / 7.5	5.7 / 7.95
IL (dB)	1.4 / 0.95	1.5 / 1.05	0.95 / 1.8	1.06 / 2.15
RL (dB)	15 / 24	> 20 / 25.5	20 / 16	17 / 13
FBW (%)	8.2 / 11	7.7 / 10.2	12.8 / 2.7	12.2 / 2.6
TZ_1	0.87 / 0.86	0.87 / 0.86	0.82 / 0.94	0.82 / 0.94
TZ_2	1.15 / 1.14	1.14 / 1.14	1.23 / 1.03	1.21 / 1.03

Specifically, in filter DB1, the lower band has been shifted from 5.3 GHz to 5.65 GHz (i.e. +6.8%) and the upper band from 7.85 GHz to 8.4 GHz (i.e. +7%), whereas in the filter DB2, the frequency shift of the lower band is from 5.25 GHz to 5.7 GHz (i.e. +8.6%) and the upper band from 7.5 GHz to 7.95 GHz (i.e. +6%). Please note that these frequency shifts are justified by the bigger spacing gaps etched on the

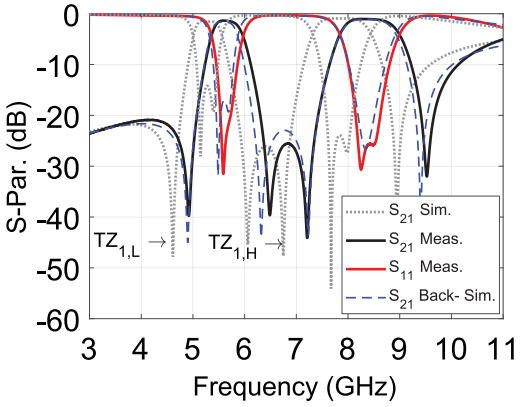

(a)

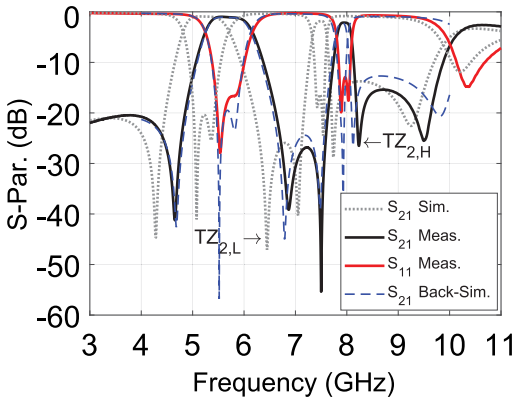

(b)

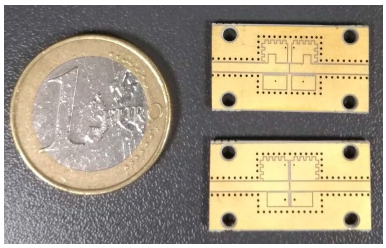

(c)

FIGURE 18. Simulations (*dotted lines*), measurements (*solid lines*) and back-simulations (*dashed lines*) for the dual-band doublets (a) of Fig 15, and (b) of Fig. 16. Naming of the TZs is also shown in order to easy readability. (c) Photograph of filter prototypes: above filter DB2, and below filter DB1.

top metal layer and the thinner finishing thickness found in all manufactured prototypes. Therefore, manufactured resonators are less loaded than simulated ones and are centered at higher frequencies.

Nevertheless, the agreement between back-simulations (that include the aforementioned systematic tolerances) and measurements is good, especially in terms of in-band IL and FBW. Finally, the positions of the TZs seem to be in good agreement with back-simulations, and just the TZs that are generated above the lower bands of both filters are slightly moved with respect to the desired frequency positions.

V. NEW FABRICATION RUN OF THE DESIGNED FILTERS

As mentioned in the previous sections, the non-vertical edges of the spacing gaps and the thinner finishing thickness found in all manufactured prototypes were responsible for the frequency shift that can be observed between 3D simulations and measurements. To fully understand such filtering response deviations, the prototypes dimensions were extensively measured by using both an optical measurement system and a stylus profilometer. Then, back-simulations were performed accounting for these prototypes deviations, and, the previous measurement responses were fully recovered, as Figs. 8-(b), 11-(b), 18-(a), and 18-(b) clearly proved.

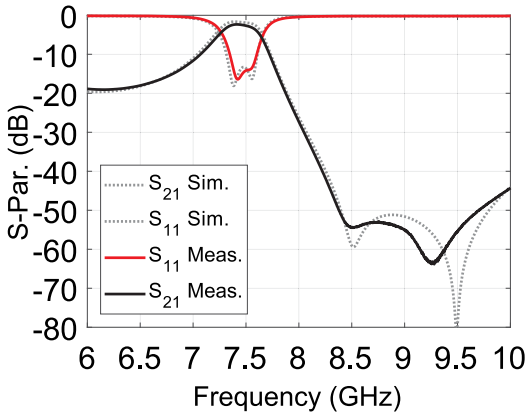

FIGURE 19. Refabricated two-pole cascaded singlets filter of Fig 7-(b): simulations (*dotted line*), and measurements (*solid lines*).

Therefore, a new fabrication run has been performed taking into account the previous results of the physical measurements of filter prototypes. Specifically, the filters of Figs. 7-(b), 12-(a), and 16 have been manufactured again by using the same PCB fabrication process, and their measurements are shown in Figs. 19, 20, and 21.

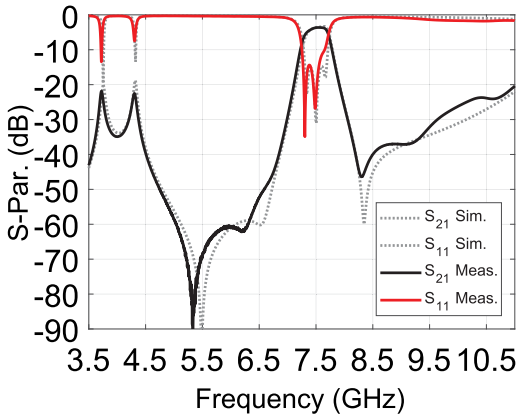

FIGURE 20. Refabricated three cascaded singlets of Fig 12-(b): simulations (*dotted line*), and measurements (*solid lines*).

The new measurements are now in excellent agreement with simulations in terms of IL, filter BWs and TZs positioning, thus fully demonstrating that enhanced selectivity, high

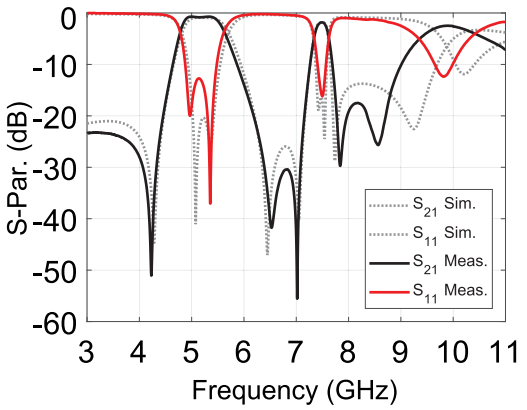

FIGURE 21. Refabricated dual-band doublet DB2 of Fig. 16: simulations (*dotted line*), and measurements (*solid lines*).

miniaturization and low-cost fabrication are easily achievable by using the proposed coaxial SIW topologies. Even if minor differences can be observed in the responses in terms of RL, the filters show RL always better than 12 dB.

VI. CONCLUSION

In this paper, a detailed study of the implementation of singlets, cascaded singlets, and dual-band doublets in coaxial SIW technology has been presented and proved by means of several BPF prototypes. Basic singlet topologies that allow the introduction of a TZ either above or below the transmission pole, are proposed and studied as a building block for implementing advanced filtering responses. Several two-pole and three-pole BPFs with two or three independent TZs were designed, fabricated and measured. The performance of these devices prove that enhanced selectivity, high miniaturization and low-cost fabrication are easily achievable by using the proposed topologies. Furthermore, the doublet concept based on a dual-mode coaxial SIW topology, and its application for the design of narrow-band and wide-band dual-band filters, have been practically demonstrated through the implementation of several compact solutions. The results clearly show that the proposed approach is suitable for the flexible design of different bandpass filters with pseudo-elliptic responses, as well as, remarkable miniaturization.

REFERENCES

[1] R. Levy, "Filters with single transmission zeros at real or imaginary frequencies," *IEEE Trans. Microw. Theory Techn.*, vol. MTT-21, no. 4, pp. 172–181, Apr. 1976.
[2] J. B. Thomas, "Cross-coupling in coaxial cavity filters-a tutorial overview," *IEEE Trans. Microw. Theory Techn.*, vol. 51, no. 4, pp. 1368–1376, Apr. 2003.
[3] J.-S. Hong and M. J. Lancaster, "Cross-coupled microstrip hairpin-resonator filters," *IEEE Trans. Microw. Theory Techn.*, vol. 46, no. 1, pp. 118–122, Jan. 1998.
[4] C.-Y. Chang and C.-C. Chen, "A novel coupling structure suitable for cross-coupled filters with folded quarter-wave resonators," *IEEE Microw. Wireless Compon. Lett.*, vol. 13, no. 12, pp. 517–519, Dec. 2003.
[5] X.-P. Cheng and K. Wu, "Substrate integrated waveguide cross-coupled filter with negative coupling structure," *IEEE Trans. Microw. Theory Techn.*, vol. 56, no. 1, pp. 142–149, Jan. 2008.
[6] X.-P. Chen, K. Wu, and Z.-L. Li, "Dual-band and triple-band substrate integrated waveguide filters with Chebyshev and quasi-elliptic responses," *IEEE Trans. Microw. Theory Techn.*, vol. 55, no. 12, pp. 2569–2578, Dec. 2007.
[7] F. Zhu, W. Hong, J.-X. Chen, and K. Wu, "Cross-coupled substrate integrated waveguide filters with improved stopband performance," *IEEE Microw. Wireless Compon. Lett.*, vol. 22, no. 12, pp. 633–635, Dec. 2012.
[8] K. Gong, W. Hong, Y. Zhang, P. Chen, and C. J. You, "Substrate integrated waveguide quasi-elliptic filters with controllable electric and magnetic mixed coupling," *IEEE Trans. Microw. Theory Techn.*, vol. 60, no. 10, pp. 3071–3078, Oct. 2012.
[9] B. Potelon, J.-F. Favennec, C. Quendo, E. Rius, C. Person, and J.-C. Bohorquez, "Design of a substrate integrated waveguide (SIW) filter using a novel topology of coupling," *IEEE Microw. Wireless Compon. Lett.*, vol. 18, no. 9, pp. 596–598, Sep. 2008.
[10] S. Sirci, F. Gentili, and J. D. Martínez, V. Boria, and R. Sorrentino, "Quasi-elliptic filter based on SIW combline resonators using a coplanar line cross-coupling," in *IEEE MTT-S Int. Microw. Symp. Dig.*, Phoenix, AZ, USA, May 2015, pp. 1–4.
[11] J. R. Montejo-Garai, "Synthesis of N-order filters with N transmission zeros at real frequencies by means of extracted poles," *Electron. Lett.*, vol. 39, no. 2, pp. 182–183, Jan. 2003.
[12] H. Joshi, H. H. Sigmarsson, D. Peroulis, and W. J. Chappell, "Highly loaded evanescent cavities for widely tunable high-Q filters," in *IEEE MTT-S Int. Microw. Symp. Dig.*, Jun. 2007, pp. 2133–2136.
[13] Y.-H. Cho and G. M. Rebeiz, "0.73–1.03-GHz tunable bandpass filter with a reconfigurable 2/3/4-pole response," *IEEE Trans. Microw. Theory Techn.*, vol. 62, no. 2, pp. 290–296, Feb. 2014.
[14] J. R. Chen, M. D. Benge, A. Anand, H. H. Sigmarsson, and X. Liu, "An evanescent-mode tunable dual-band filter with independently-controlled center frequencies," in *IEEE MTT-S Int. Microw. Symp. Dig.*, May 2016, pp. 1–4.
[15] S.-W. Wong *et al.*, "Individually frequency tunable dual-and triple-band filters in a single cavity," *IEEE Access*, vol. 5, pp. 11615–11625, 2017.
[16] S. Amari, U. Rosenberg, and J. Bornemann, "Singlets, cascaded singlets, and the nonresonating node model for advanced modular design of elliptic filters," *IEEE Microw. Wireless Compon. Lett.*, vol. 14, no. 5, pp. 237–239, May 2004.
[17] S. Bastioli, "Nonresonating mode waveguide filters," *IEEE Microw. Mag.*, vol. 12, no. 6, pp. 77–86, Oct. 2011.
[18] M. Esmaeili and J. Bornemann, "Substrate integrated waveguide triple-passband dual-stopband filter using six cascaded singlets," *IEEE Microw. Wireless Compon. Lett.*, vol. 24, no. 7, pp. 439–441, Jul. 2014.
[19] C. Tomassoni, L. Silvestri, M. Bozzi, and L. Perregrini, "Quasi-elliptic SIW band-pass filter based on mushroom-shaped resonators," in *Proc. 45th Eur. Microw. Conf. (EuMC)*, Sep. 2015, pp. 749–752.
[20] S. Amari, U. Rosenberg, and J. Bornemann, "Adaptive synthesis and design of resonator filters with source/load-multiresonator coupling," *IEEE Trans. Microw. Theory Techn.*, vol. 50, no. 8, pp. 1969–1978, Aug. 2002.
[21] P. Chu *et al.*, "Dual-mode substrate integrated waveguide filter with flexible response," *IEEE Trans. Microw. Theory Techn.*, vol. 65, no. 3, pp. 824–830, Mar. 2017.
[22] S. Sirci, M. A. Sánchez-Soriano, J. D. Martínez, and V. E. Boria, "High selectivity filters in coaxial SIW based on singlets and doublets," in *IEEE MTT-S Int. Microw. Symp. Dig.*, Philadelphia, PA, USA, Jun. 2018, pp. 1–4.
[23] M. A. Sánchez-Soriano, S. Sirci, J. D. Martínez, and V. E. Boria, "Compact dual-mode substrate integrated waveguide coaxial cavity for bandpass filter design," *IEEE Microw. Wireless Compon. Lett.*, vol. 26, no. 6, pp. 386–388, Jun. 2016.
[24] S. Amari and U. Rosenberg, "Characteristics of cross (bypass) coupling through higher/lower order modes and their applications in elliptic filter design," *IEEE Trans. Microw. Theory Techn.*, vol. 53, no. 10, pp. 3135–3141, Oct. 2005.
[25] J. D. Martínez, S. Sirci, M. Taroncher, and V. E. Boria, "Compact CPW-fed combline filter in substrate integrated waveguide technology," *IEEE Microw. Wireless Compon. Lett.*, vol. 22, no. 1, pp. 7–9, Jan. 2012.
[26] S. Sirci *et al.*, "Design and multiphysics analysis of direct and cross-coupled SIW combline filters using electric and magnetic couplings," *IEEE Trans. Microw. Theory Techn.*, vol. 63, no. 12, pp. 4341–4354, Dec. 2015.

[27] J. D. Martínez, S. Sirci, V. E. Boria, P. Martín-Iglesias, and H. Leblond, "Practical considerations on the design and optimization of substrate integrated coaxial filters," in *Proc. IEEE MTT-S Int. Conf. Numer. Electromagn. Multiphys. Modeling Optim. RF, Microw., THz. Appl. (NEMO)*, Seville, Spain, May 2017, pp. 299–301.
[28] A. Anand and X. Liu, "Reconfigurable planar capacitive coupling in substrate-integrated coaxial-cavity filters," *IEEE Trans. Microw. Theory Techn.*, vol. 64, no. 8, pp. 2548–2560, Aug. 2016.
[29] G. Matthaei, L. Young, and E. M. T. Jones, *Microwave Filters, Impedance-Matching Networks, and Coupling Structures*, 1st ed. New Jersey, NJ, USA: Artech House, 1980.
[30] D. Deslandes and K. Wu, "Analysis and design of current probe transition from grounded coplanar to substrate integrated rectangular waveguides," *IEEE Trans. Microw. Theory Techn.*, vol. 53, no. 8, pp. 2487–2494, Aug. 2005.
[31] M. A. Sánchez-Soriano, S. Sirci, J. D. Martínez, and V. E. Boria, "Compact bandpass filters based on a new substrate integrated waveguide coaxial cavity," in *Proc. IEEE MTT-S Int. Microw. Symp. Dig.*, San Francisco, CA, USA, May 2016, pp. 1–4.
[32] A. P. Saghati, A. P. Saghati, and K. Entesar, "Ultra-miniature SIW cavity resonators and filters," *IEEE Trans. Microw. Theory Techn.*, vol. 63, no. 12, pp. 4329–4340, Dec. 2015.

STEFANO SIRCI (S'13–M'17) received the B.S. and M.S. degrees (Hons.) from the University of Perugia, Perugia, Italy, in 2006 and 2009, respectively, and the Ph.D. degree from the Universitat Politècnica de València, Valencia, Spain, in 2017, all in electronic engineering, where he is currently with the Microwave Application Group, Institute of Telecommunications and Multimedia Applications, as a Postdoctoral Research Associate, involved in RF passive hardware design.

He has collaborated in research projects supported by the Spanish Government, the European Space Agency, and private companies. His research interests include the analysis, design, and integration of microwave passive components with advanced filtering responses (reconfigurable and quasi-elliptic filters) with emphasis on planar, substrate integrated waveguide, and coaxial SIW topologies in PCB and LTCC technologies.

Dr. Sirci serves as a Reviewer for various journals and conferences, including the IEEE Transactions on Microwaves, Theory and Techniques, the IEEE Microwave and Wireless Components Letters, the IEEE Access, and the *IET Microwaves, Antennas and Propagation*.

MIGUEL ÁNGEL SÁNCHEZ-SORIANO (S'09–M'13) was born in Yecla, Murcia, Spain, in 1984. He received the Telecommunications Engineer degree (with a Special Award) and the Ph.D. degree in electrical engineering from Miguel Hernández University, Spain, in 2007 and 2012, respectively, where he joined the Radiofrequency Systems Group, as a Research Assistant, in 2007.

He was a Visiting Researcher with the Microwaves Group, Heriot-Watt University, Edinburgh, U.K., in 2010. In 2013, he joined the LabSTICC Group, Université de Bretagne Occidentale, Brest, France, as a Postdoctoral Researcher, where he worked for two years. In 2015, he was a Juan de la Cierva Research Fellow with the Microwave Application Group, Universitat Politècnica de València, Valencia, Spain. Since 2015, he has been an Assistant Professor with the University of Alicante. His research interests include the analysis and design of microwave planar devices, especially filters and their reconfigurability, and the multiphysics study of high-frequency devices.

Dr. Sánchez-Soriano was a recipient of the runner-up HISPASAT Award for the Best Spanish Doctoral Thesis in New Applications for Satellite Communications, awarded by the Spanish Telecommunication Engineers Association (COIT/AEIT), and of the Extraordinary Ph.D. Award from the Miguel Hernández University. He serves as an Associate Editor for the journals, including the IEEE Transactions on Microwaves, Theory and Techniques, and the *IET Microwaves, Antennas and Propagation*, and as a Regular Reviewer for more than ten journals and several IEEE international conferences, including the IEEE Microwave and Wireless Components Letters, the IET Electronics Letters, and the IEEE Access.

JORGE DANIEL MARTÍNEZ (M'09) was born in Murcia, Spain, in 1979. He received the Telecommunication Engineering and Ph.D. degrees in electrical engineering from the Universitat Politècnica de València (UPV), Valencia, Spain, in 2002 and 2008, respectively, where he joined the Department of Electronic Engineering, as a Research Fellow, in 2002.

He was a Visiting Researcher with XLIM CNRS-Université de Limoges, France, in 2007, working on the design and fabrication of RF MEMS components under the advice of Prof. P. Blondy. Since 2009, he has been an Assistant Professor with UPV, belonging to the I3M R&D Institute and actively collaborating with the Microwave Applications Group, UPV. He is currently a Technical Responsible of the Laboratory for High Frequency Circuits Fabrication, UPV, focused on low temperature co-fired ceramics and other related multi-layered technologies. His current research interests include emerging technologies for reconfigurable microwave components with emphasis on tunable filters and RF MEMS, the design and fabrication of advanced microwave filters in planar and substrate integrated waveguide technologies, and the application of multi-layer fabrication technologies to RF/microwave and millimeter-wave applications.

VICENTE E. BORIA (S'91–A'99–SM'02–F'18) was born in Valencia, Spain, in 1970. He received the Ingeniero de Telecomunicación (Hons.) and the Doctor Ingeniero de Telecomunicacién degrees from the Universitat Politècnica de València, Valencia, in 1993 and 1997, respectively, where he joined the Departamento de Comunicaciones, in 1993, and has been a Full Professor, since 2003.

In 1995 and 1996, he held a Spanish Trainee position with the European Space Research and Technology Centre, European Space Agency, Noordwijk, The Netherlands, where he was involved in the area of EM analysis and design of passive waveguide devices. He has authored or co-authored ten chapters in technical textbooks, 180 papers in refereed international technical journals, and over 200 papers in international conference proceedings. His current research interests include the analysis and automated design of passive components, left-handed and periodic structures, and the simulation and measurement of power effects in passive waveguide systems.

Dr. Boria has been a member of the IEEE Microwave Theory and Techniques Society (IEEE MTT-S) and the IEEE Antennas and Propagation Society, since 1992. He is also a member of the Technical Committees of the IEEE-MTT International Microwave Symposium and of the European Microwave Conference. He acts as a Regular Reviewer of the most relevant IEEE and IET technical journals on his areas of interest. He currently serves as an Associate Editor for the IEEE Microwave and Wireless Components Letters and the *IET Electronics Letters*, and as an Editorial Board Member for the *International Journal of RF and Microwave Computer-Aided Engineering*.